

FORM-FINDING OF A GRID SHELL IN COMPOSITE MATERIALS

C. DOUTHE, O. BAVEREL, J.-F. CARON

Institut Navier – LAMI, Ecole Nationale des Ponts et Chaussées
6 et 8, avenue Blaise Pascal - Champs-sur-Marne - F-77455 Marne-la-vallée cedex 2
douthe@lami.enpc.fr, baverel@lami.enpc.fr, caron@lami.enpc.fr

Editor's Note: Manuscript submitted 19 September 2005; revision received 3 March 2006; accepted for publication 5 March 2006. This paper is open for written discussion, which should be submitted to the IASS Secretariat no later than December 2006.

SUMMARY

The advantages of the use of glass fiber composites for grid shell are presented. The shape of grid shells results from a post-buckling state of tubes. To bypass the difficulty to predict the geometry of the final equilibrium state, the large rotations which occur during the erection process are modelled using the dynamic relaxation algorithm. This paper proposes an adaptation of this method for structures prestressed by bending through the development of a computer program. It includes the validation of this numerical tool through comparisons with a finite elements software. Then an application to the form-finding of a grid shell and the study of its stability under standard loading conditions will be presented. Finally the authors conclude on the technical and economic feasibility of this composite grid shell.

Keywords: Composite material, Dynamic relaxation, Grid shell, form-finding, non-linear analysis.

1. INTRODUCTION

In the last twenty years many applications of composite materials in the construction industry were made. The main field of application concerns the reinforcement of concrete beams with carbon fiber plates [1] or post tension cables. But more recently, a footbridge with carbon fiber stay-cable was build in Laroin (France, 2002), another footbridge, all made of glass fiber composite, was build in Aberfeldy (Scotland, 1993) and a movable bridge (the Bonds Mill lift bridge in Stonehouse, England, 1995). Nevertheless applications using composite materials as structural elements remain exceptional in comparison with concrete, steel or even wood. Although the qualities of their mechanicals properties are obvious (low density, high strength and high resistance against corrosion and fatigue), their relatively low elastic modulus make their use in usual buildings more expensive than other traditional materials. In order to take advantages on every characteristic of composite materials, new structural concepts must be found.

The LAMI-ENPC is therefore developing a project of innovating footbridge [2] and an experimental grid shell. This last project takes place in the

framework of a research on structures for shelters for temporary or permanent purposes [3]. Its structural analysis was first presented in CCC2005 [4] and will be detailed in this paper. Four design principles guided the conception stage of this experimental grid shell:

- Optimal use of the mechanical characteristics of the fibers;
- Simple connection between components of the structure;
- Optimal design according to its use;
- Cheap material cost toward use of components already available in the industry.

2. GRID SHELLS

2.1. Definition of grid shells

The name of grid shell commonly describes a structure with the shape and strength of a double-curvature shell, but made of a grid instead of a solid surface. These structures can cross large span with very few material. They can be made of any kind of material - steel, aluminium, wood or even cardboard tubes... Generally, the metallic structures are made of short straight elements defining a facet

geometry. The complexity of this geometry requires the development of many clever and expensive assemblies. To mitigate this disadvantage, a very specific erection process was developed that uses the ability of slender components to be bent. Long continuous bars are assembled on the ground, pinned between them in order to confer on the grid a total absence of plane shear rigidity which will allow large deformations. The grid is deformed elastically by bending until the desired form is obtained and then rigidified. Three grid shells were built in the world using this method: the Mannheim Budesgartenshau (Frei Otto, 1975), the Weald and Downland Museum (E. Cullinan, Happold, 2002) [5] and the Japanese pavilion for the Hanover 2000 Exhibition (Shigeru Ban, Happold). The structure of the first two grid shells is made of wooden bars, while that of the third one uses cardboard tubes, locally reinforced with wooden arches.

2.2. The choice of the material

In this process of assembly, initial bending strains are induced in the element of the lattice structure. In the existing grid shells, wood was chosen because of its low density and high limit strain (about 2%) but not for its strength (30 MPa at best). Glass fiber reinforced polymer (GFRP) exhibits a strength of about 350 MPa and a limit strain of about 1.5% for only 1.9 kg/m³. Glass fiber reinforced polymers have therefore much higher rigidities (from 20 GPa to 40 GPa) than wood (around 10 GPa), so that, for a given geometry of grid shell, the buckling load of a composite grid shell will be higher than for a wooden grid shell. These mechanical properties make thus the use of GFRP very attractive for this kind of application.

As the stresses in the beams are almost exclusively axial stresses, fibers are required only in the main direction of the beam. Therefore the industrial process of pultrusion would provide a cost-effective method for the production of unidirectional composite materials. It will also allow the production of very long tubes that would avoid the problem of joining the wood cleats. To improve the performance of the section of the tube, one could also choose a circular pull-winded tube with fiber perpendicular to the axis of the tube. It will raise the limit strength and avoid the ovalization of the section, but it will also raise the cost of the material production of about 15% in comparison with the pultrusion process.

Moreover with standard diameters of tubes, standard swivel scaffolding elements (see figure 1) already available in the industry could be used for the realization of the connection between the tubes. Hereby the material cost can be once again very effective. This is why these technical solutions seems to be appropriate for the construction of grid shells, and could contribute to the development of this type of structures.



Figure 1: Standard swivel scaffolding elements

2.3. The existing form-finding methods

In grid shells structure, the elastic strain of the phase of assembly imposes large displacements on the beams and induces thereafter a state of bending prestress. The search for stable and aesthetic forms (the so called form-finding step), the evaluation of strains and the optimization of their distribution in the various elements require taking into account those large displacements and being able to model strong non-linearity.

The grid shell of Mannheim of 1975 was conceived by inversion of a cable net subjected to its own weight as shown in [6] and by work on equivalent small scale models. This method was only a first approach of the form of grid shells because the reverse hanging method leads to simple compression stresses whereas, in grid shell, the initial state of stresses combines bending, compressive and tensile stresses.

Today, the power of computer has considerably increased and the calculation can be carried out using finite element methods. However, usual algorithms (Newton-Raphson for instance) quickly present significant computing times and problems of convergence due to the high level of rotation and displacement. These difficulties of the modeling of a form-finding step not only concern grid shells, but also a various type of structures among which tensile structures. For this type of structures, two

specific methods were developed and are today widely used in Europe: firstly the force density method [7] and its extension to a continuous geometry, the surface stress density method [8] and secondly the dynamic relaxation method. This method is the only one that was extended to the form-finding of grid shell and will be thus developed below.

3. THE DYNAMIC RELAXATION METHOD

3.1. History

The dynamic relaxation method was developed by A. S. Day studying marine streams. In this original technical solution, static equilibrium is regarded as the limit equilibrium condition of strongly damped vibrations. The first application to tensile structures and hanged roofs was carried out by Day [9]. Then came the works of M.R. Barnes on form-finding and his first applications to prestressed cable nets [10], to membranes and inflatable structures [11], and to structures with bending rigidity and to grid shells [12]. One can also easily find other examples of complex structures calculated by dynamic relaxation like cable-domes [13]. Today this method has been applied to many fields of mechanics, such as for example a study on metallic foams performed in the ENPC and the Navier Institute [14].

“The basis of the method is to trace step-by-step for small time increments, the motion of each node of a structure until, due to artificial damping, the structure comes to rest in a static equilibrium.” [11]. In the original version of the DR method, a parameter of viscous damping proportional to the speed and the mass of the nodes was used. But to ensure the convergence of the process, it was necessary to introduce controls and adjustments on those various parameters [15]. This method remains relatively delicate to implement, so that an alternative procedure of kinetic damping will be preferred in this paper. Kinetic damping is an artificial damping whose principle relies on the exchange during the movement, for a conservative system, between kinetic energy and potential elastic energy which one seeks the minimum. In this procedure, the oscillations of the structure start from an arbitrary geometry and are free until a maximum of kinetic energy is reached. The structure is then stopped: all speeds are given artificially to zero. Then the structure is again free

to oscillate to the next maximum of kinetic energy where, like previously, speeds are given to zero. And so on, until the kinetic energy of all the modes of vibrations is dissipated.

3.2. Modeling the movement of the structure

The initial grid is made of long continuous beams. They are set up in two principal directions with a regular spacing between them. These beams follow an Euler-Bernoulli model and their behavior is linear elastic. The beams in one direction are pinned with the beams in the other direction of the grid so that there are no bending stresses induced by the connection. No external bending moment is applied. The beams are thus subjected only to shear and normal forces. One can then show by considerations of structural mechanics, that there is no torsion in initially straight beam under such a load if its principal inertias are equals [12]. Each beam is thus modeled like a tube of Young modulus E , inertia I and section S . Each node of a beam has three translational degrees of freedom so that the position of node i will be noted by the vector \underline{X}_i .

The calculations start from an arbitrary geometry. In this initial state, the system is unstable and will move under the actions of the internal stresses and external loads. The internal stresses in the current geometry are computed using the stress free state of the structure. To describe the movement, the position of every node is calculated for each time-step Δt until balance.

First consider that the position \underline{X}_i^t of every node i at time t is known and that their speed $\underline{V}_i^{t-\Delta t/2}$ at time $t-\Delta t/2$ is known too. The acceleration \underline{y}_i^t at node i and time t is given by the second law of Newton (1) from the resultant \underline{R}_i^t of all forces applied to node i and from its mass m_i .

$$\underline{R}_i^t = m_i \cdot \underline{y}_i^t \quad (1)$$

To go up to the speed $\underline{V}_i^{t+\Delta t/2}$ of node i at time $t+\Delta t/2$, a centered approximation scheme is used for the acceleration, so that one can deduce the expression of the speed according to (2).

$$\underline{V}_i^{t+\Delta t/2} = \underline{V}_i^{t-\Delta t/2} + \frac{\Delta t}{m_i} \cdot \underline{R}_i^t \quad (2)$$

Using again a centered approximation, one obtains (3) the position $\underline{X}_i^{t+\Delta t}$ of node i at time $t+\Delta t$:

$$\underline{X}_i^{t+\Delta t} = \underline{X}_i^t + \Delta t \cdot \underline{V}_i^{t+\Delta t/2} \quad (3)$$

From the new positions $\underline{X}_j^{t+\Delta t}$ of all the nodes j connected to node i , one can then calculate the internal forces $\underline{F}_i^{\text{int}}$ at node i and time $t+\Delta t$, add to them the external load $\underline{P}_i^{\text{ext}}$ and so define the resultant $\underline{R}_i^{t+\Delta t}$ (4) of the forces applied to node i at time $t+\Delta t$.

$$\underline{R}_i^{t+\Delta t} = \underline{P}_i^{\text{ext}} + \sum_j \underline{F}_{i,j}^{\text{int}}(\underline{X}_i^{t+\Delta t}, \underline{X}_j^{t+\Delta t}) \quad (4)$$

At the boundary, the displacements are constrained, but not the rotations. The compatibility of the movement with the boundary conditions is ensured at each step during the calculation of speeds, by setting certain components to zero. This verification was chosen because it allows computing directly the kinetic energy on compatible speeds.

3.3. Internal forces

Internal forces in a beam are of two natures: traction-compression and bending. The modeling presented hereafter adopts that proposed by M. R. Barnes [11], extends it to a three dimensional problem and to a more sophisticated modeling of connection between the elements.

Axial stresses

Let us first consider the diagram of figure 2 of a portion of an arch constituted of three nodes ($i-1$, i and $i+1$).

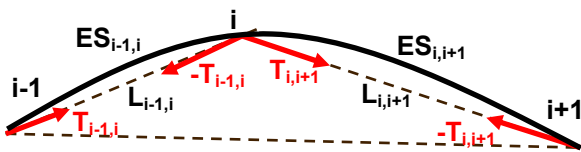


Figure 2: Scheme of the axial stresses

At each current node i of a beam, there are two forces of compression-traction $\underline{T}_{i-1,i}^t$ and $\underline{T}_{i,i+1}^t$ related to the two connected elementary beams. At time t , these forces are calculated for each elementary beam according to its stiffness $ES_{i,j}$ (where j stands for $i-1$ or $i+1$), and to the axial strain of the centroid of the beam $\varepsilon_{i,j}^t$ (5).

$$\underline{T}_{i,j}^t = ES_{i,j} \cdot \varepsilon_{i,j}^t \quad (5)$$

One can then deduce the deformation $\varepsilon_{i,j}^t$ from the length of the beam $L_{i,j}^0$ in the stress-free geometry, its length $L_{i,j}^t$ at time t and the position \underline{X}_{i+1} and \underline{X}_{i-1} of the two adjacent nodes. Their expression is given in (6), where $\underline{X}_{i,j}^t$ denotes the relative position $\underline{X}_j - \underline{X}_i$ and $L_{i,j}$ its norm.

$$\underline{T}_{i,j}^t = ES \cdot \left(\frac{1}{L_{i,j}^0} - \frac{1}{L_{i,j}^t} \right) \cdot \underline{X}_{i,j}^t \quad (6)$$

For the calculation of cable elements, one can easily introduce non linearity by not tacking into account the force in the cable if it is subjected to compression.

Bending stresses

For the calculation of bending stresses, let us first make the assumption that three successive nodes of a beam are always sufficiently close so that one can suppose that they are on a circle of radius ρ_i^t (see figure 3).

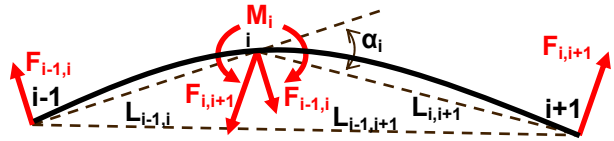


Figure 3: Scheme of bending stresses

This radius will be regarded as the radius of curvature at node i and time t . It can be calculated from the positions of the three nodes (7), where $\sin \alpha_i^t$ is given by (8):

$$\rho_i^t = \frac{L_{i-1,i+1}^t}{2 \cdot \sin \alpha_i^t} \quad (7)$$

$$\text{with } \sin \alpha_i^t = \left\| \frac{\underline{X}_{i-1,i}^t \wedge \underline{X}_{i,i+1}^t}{L_{i-1,i}^t \cdot L_{i,i+1}^t} \right\| \quad (8)$$

Then, from the mechanics of materials, one deduces the bending moment M_i^t at node i and at time t (9):

$$M_i^t = \frac{EI_i}{\rho_i^t} \quad (9)$$

The direction of the bending moment is perpendicular to the local plane of curvature that is

given by the cross product $\underline{X}_{i-1,i}^t \times \underline{X}_{i,i+1}^t$ so that the final expression of the bending moment \underline{M}_i^t is (10).

$$\underline{M}_i^t = \frac{2 \cdot EI_i}{L_{i-1,i+1}^t} \cdot \frac{\underline{X}_{i-1,i}^t \wedge \underline{X}_{i,i+1}^t}{L_{i-1,i}^t \cdot L_{i,i+1}^t} \quad (10)$$

For more convenience, this bending moment \underline{M}_i^t will be transformed into equivalent forces applied to the nodes. Therefore let us consider the right-hand side of the beam. If the reaction $\underline{F}_{i-1,i}^t$ at node $i-1$ is assumed to be perpendicular to $\underline{X}_{i-1,i}^t$, one can deduce from the balance of the forces due to the moment \underline{M}_i^t the value of $\underline{F}_{i-1,i}^t$ (11).

$$\underline{F}_{i-1,i}^t = \frac{\underline{X}_{i-1,i}^t \wedge \underline{M}_i^t}{L_{i-1,i}^t{}^2} \quad (11)$$

In the same way, the balance of the left hand-side gives $\underline{F}_{i,i+1}^t$ (12).

$$\underline{F}_{i,i+1}^t = \frac{\underline{X}_{i,i+1}^t \wedge \underline{M}_i^t}{L_{i,i+1}^t{}^2} \quad (12)$$

And so the moment \underline{M}_i^t at node i is broken up into a set of four forces directly connected to the current geometry of the beam. Two are applied to node i , one to node $i+1$ and one to node $i-1$.

If the structure studied is a plane structure that is loaded in its plane, beams with initial curvature can be modelised by taking it into account in the expression (9) of the bending moment. But if the problem is not plane, the introduction of beams that are not initially straight will invalidate the assumption that no torsion appears. It will be then necessary to introduce a rotational degree of freedom at every node. An advantage of this modification will be that it would allow the modeling of beams with different inertia in the two principal directions. It would also make the algorithm more versatile for the study of prestressed structures in large displacements and rotations taking into account the lateral torsional buckling.

3.4. Efforts at connection points

At connection points, there is an interaction between beams. To model this interaction, one defines separately, at any connection point, a node on each beam. The connection element has a

thickness that induces an eccentricity between those nodes. If these eccentricities act as geometrical imperfections, one can expect a great loose of resistance of the structure. However in these first calculations, the eccentricities between the axes of the beams will be neglected and it will be assumed that the connected nodes have the same spatial position. Then, according to the method exposed higher, one calculates the internal forces associated to the current geometry for each beam separately. It is considered that the total force applied to each node is the sum of the internal forces of each node. Initially at the same spatial position, the nodes of the various beams are subjected to identical forces at every time, they thus remain at the same spatial position.

3.5. Stability and convergence

To accelerate the speed of convergence, so that the system evolves faster to its position of equilibrium, one can increase the time step or decrease the nodal fictitious masses. Nevertheless, when the time step exceeds a certain breaking value or the fictitious nodal masses become too low, numerical instabilities appear. The phenomenon is explained simply in [10]. The generalization of the problem to a system of beams, at every moment requires the knowing of the total stiffness corresponding to the various efforts being applied to the node. For a current beam, the ratio EI/ES is about 1/100 so that, in a first approach, the bending stiffness can be neglected in comparison to the tension stiffness. Thus, at the beginning of the calculation of a peak, the fictitious masses m_i^t are fixed according to the total axial stiffness of the beams connected to the node i and can be written as (13):

$$m_i^{peak} = \lambda \cdot \frac{\Delta t^2}{2} \cdot \sum_j \left(\frac{ES}{L^0} + \frac{T^{peak}}{L^0} \right)_{i,j} \quad (13)$$

In this expression, λ is a parameter slightly higher than 1 that insures the stability of the algorithm and an acceptable time of convergence. $(ES/L)_{i,j}$ represents the axial elastic stiffness and $(T/L)_{i,j}^t$ the geometric stiffness of each elementary beam. $T_{i,j}^t$ is the current tension in the beam which is calculated according to the axial elastic stiffness and the current strain of the element at time t . To accelerate convergence, the fictitious masses are reset at every energy peak according to the current geometric stiffness.

4. VALIDATION OF THE PROGRAM

The dynamic relaxation algorithm of section 3 was implemented in a free scientific software package named Scilab™ [16], developed in common by the ENPC (Ecole Nationale des Ponts et Chaussées) and the INRIA (Institut National de Recherche en Informatique et Automatique). The 2D-validation comprises several tests:

- checking of the stability of the algorithm;
- convergence of the results and influence of the number of elements;
- comparison of the results with those obtained with the finite element method using Abaqus™.

4.1. 2D-Validation

The “elastica” (the post-buckled curve of a pin-ended beam) provides a useful comparison because there is an analytical expression of the deformed shape of the beam (Euler 1744). The numerical test example is a tubular straight beam of 12 m length, 50 mm diameter and 2 mm thickness with a Young modulus of 35 GPa. The beam, supported on end rollers and restrained to lie in the plane xz, is subjected to opposite end axial loads of 1000 N that will cause the looping of the beam (see figure 4).

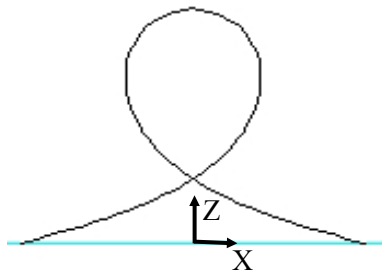


Figure 4: Buckled beam

For the dynamic relaxation algorithm, the Euler-Bernoulli model of section 3 is implemented. For the finite elements method (FEM), an elastic Timoshenko’s model of beam with 6 degrees of freedom per node was chosen. The geometrical non-linearity solver implemented is the Newton-Raphson method.

The first aim of this validation is to compare the results for the dynamic relaxation (DR) model and the FEM. The second aim is to test the influence of the discretization for the DR model. Note that for

the FEM, the reference values are the results of the beam divided in 100 elements and that for the DR, the number of elements of the beams vary from 10 to 100. The whole results are presented in table 1. The maximal displacements U_x and U_z are in cm, the normal forces in N and the maximal bending moment M_{max} in N.m.

Model	Nb of elem.	$U_{x_{max}}$ (cm)	$U_{z_{max}}$ (cm)	N_{min} (N)	N_{max} (N)	M_{max} (Nm)
DR	10	3,566	8,614	-968	728	3 460
	20	3,552	8,421	-968	947	3 451
	30	3,52	8,409	-969	974	3 451
	40	3,512	8,40	-969	979	3 447
	50	3,513	8,394	-969	992	3 445
	100	3,513	8,384	-969	999	3 440
FEM	100	3,512	8,38	-969	999	3 441
theory	Cont.	3,46	8.42			3460

Table 1: Results comparison (2D)

Table 1 shows that the results of the model are very close from those obtained with the finite element method (less than 1‰ error). The differences that remain between the analytical continuous model and the two others are due to the fact that the numerical models take into account the strain energy related to normal forces and not only to the bending moment. The table shows also that the DR-model provides accurate enough results (less than 3% error) with only 20 elements.

Nb of element	DR		FEM	
	Time (sec)	Nb of iter.	Time (sec)	Nb of iter.
10	28	3374	36	57
20	112	7580	35	58
30	256	12084	35	59
40	442	15409	36	62
50	681	19779	37	66
100	3502	50592	41	70

Table 2: Computing time comparison (2D)

On this elementary problem, the comparison of the computing times between the two methods (see table 2) shows that dynamic relaxation requires much more time than the finite element method. Actually for the dynamic relaxation, the buckling movement is very long to initiate as it can be seen on the history of the kinetic energy in figure 5. To improve the computing times, it is necessary to

choose an initial geometry that is not too far away from the equilibrium geometry. In this particular case a parabola of about 3.5 m height and 12 m length provides much better computing times (4562 iterations in 108 seconds) for the same precision.

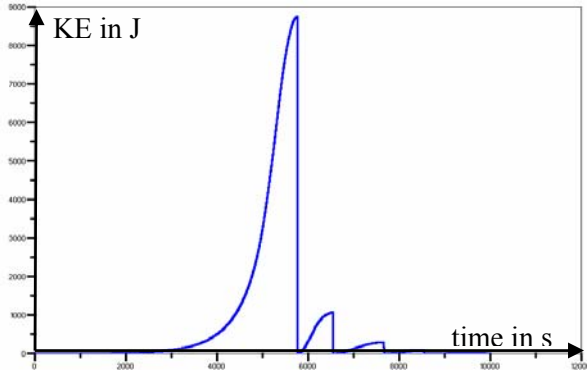


Figure 5: History of the kinetic energy

4.2. 3D-Validation

The 3D validation is based on a square grid of beams, five in each direction x and y (see figure 6). The beams are the same as for the 2D-validation: tubular straight beams of 12 m length, 50 mm diameter and 2 mm thickness with a Young modulus of 35 GPa. The distance between two successive beams is 2 m. The beams are supported on end rollers and loaded upwards at every connection point with 200 N. At connection point, the rotations between the beams are free.

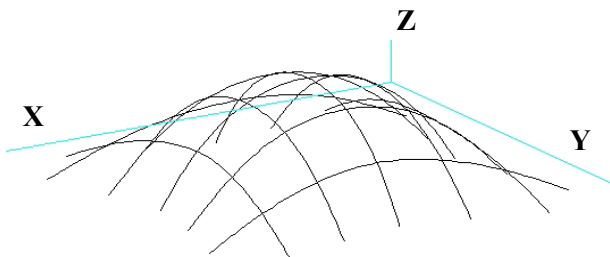


Figure 6: Post-buckled grid

As for the 2D-validation, the Euler-Bernouilli model of section 3 is implemented for the dynamic relaxation algorithm. And for the finite element model, an elastic Timoshenko’s beam element with 6 degrees of freedom per node was chosen and the geometrical non-linear solver is again the Newton-Raphson method.

The convergence of the DR algorithm was tested by changing the number of elements of the each beam from 6 to 60. During the tests, the maximum displacements were measured in every direction (U_x and U_z ; as the problem is symmetrical, $U_x = U_y$) and the maximum reactions R_z . Results are presented below in table 3. Once again the results of the dynamic relaxation model are very close from those obtained with the finite element method (less than 1% error). Like previously, it is remarkable that this accuracy can be obtained with very few elements (24 elements).

Model	Nb of elem.	$U_{x_{max}}$ (in m)	$U_{z_{max}}$ (in m)	$R_{z_{max}}$ (in N)
DR	6	1,42	3,41	434
	12	1,37	3,33	450
	24	1,35	3,3	458
	60	1,34	3,29	458
FEM	60	1,36	3,31	459

Table 3: Results comparison (3D)

Looking now to the results of table 4, the conclusion of the comparison of the computing time between the two methods is not as obvious as in the two dimensional case. Actually for 60 elements the finite element method still converges faster than the dynamic relaxation. But one can observed that the FEM had great difficulties to converge for a smaller number of elements, where the DR-model still has quick convergence.

Nb of elements	DR		FEM	
	Time (sec)	Nb of iter.	Time (sec)	Nb of iter.
6	61	1086	$>3.10^5$	$>10^6$
12	345	3840	$>2,5.10^5$	$8,5.10^5$
24	938	5520	$>1,5.10^5$	7.10^5
60	7572	18392	188	287

Table 4: Computing time comparison (3D)

In the same way, if the loading is doubled to 400 N per node (in the 24 elements per beam model), the computing time of the FEM goes over 40 hours where the computing time of the DR remains quite equal to that obtain for 200 N per node (3968 iterations in 674 seconds). Thus, it can be concluded that the DR provides accurate results and is much less sensitive than the common Newton-Raphson Method used for the FEM.

To complete this study, the geometry of this grid shell was compared to the geometry of a hanging net with the same initial pattern submitted to its own weight. The geometric characteristics of the cables are the same as that of the bars. The boundary conditions of the hanging net are those of the results of the form-finding step of the associated grid shell. It is found that the average gap between the two configurations is of about 70 mm with a standard deviation of 115 mm. The maximum error made on the vertical position of a node is about 6%. So, if one considers that the errors on the positions of the nodes have very important consequences on the conception of the cladding, the effect of the bending rigidity shall not be neglected for the calculations of grid shells.

5. STUDY OF A GRID SHELL

5.1. Description of the structure

The grid shell presented here in figure 7 is made from an orthogonal grid of circular hollow beams of 50 mm diameter and 2 mm thick. The space between two consequent beams is about 0.75 m. In the initial state the perimeter of the grid is made of two semi-circles of radius 7 m separated by a rectangle of 14 m length and 6 m width (figure 7).

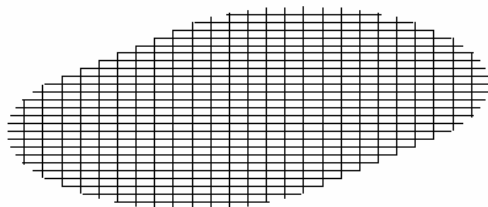


Figure 7: Initial state of the grid

The grid is then deformed elastically. It is pushed upwards at every connecting node and submitted to horizontal forces all around the boundaries in the initial plane of the grid. These actions provoke a global buckling of the grid and a shortening of the length of the grid shell. Once an aesthetic form is reached, the extremities of the beams are fixed to the ground with free rotations. The final form of the grid shell is in equilibrium with prestresses due to the bending in the beams and the actions of supports. The form-finding of the structure is yet to the end, the grid shell can be stabilized (figure 8) with, in our example, steel cables of 5 mm diameter in order to give it a shell like behaviour.

The characteristics of the grid shell in its final form are presented below:

Height:	5.80 m;
Width:	13.0 m;
Length:	13.5 m;
Total length of beam:	670 m;
Total length of cables:	900 m;
Number of connections:	463;
Livable surface (h>1.8m):	72 m ² ;
Surface of the envelope:	225 m ² ;
Weight of the structure:	8.5 kg/m ² ;
Ratio thickness/Span:	1/270.

These last two characteristics have to be compared with standard steel shed which structural weight is about 20 kg/m² and which ratio thickness per span relies by 1/25. Grid shell are thus very light and extremely thin structures. Therefore their behavior under external loads has to be investigated.

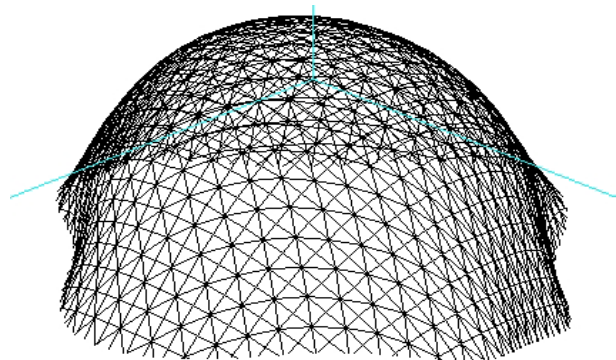


Figure 8: Final shape of the grid shell

5.2. Test under climatic action

The grid shell was tested numerically when it is subjected to snow and wind load. The calculations were done with the DR program that performed here the non-linear analysis of the structure and predicts its instability. The values of climatic actions are taken from the Eurocode 1. The grid shell is virtually located next to the ENPC in Paris, so that the wind pressure will be taken equal to 780 Pa and the reference snow load to 36 kg/m². To compute the different pressure coefficients, it is assumed that the geometry of the grid shell is closed to that of a spherical dome.

Several directions of wind were tested in order to choose the direction that implies the largest deflection of the grid shell. The worst condition is an angle of 45° with principal directions of the grid. A service limit state (SLS) combination of actions is calculated with the chosen wind load and the associated anti-symmetric distribution of snow.

In some primary tests the importance of the cables stiffness was observed. With the chosen diameter of the cables, the deformations of the grid shell are acceptable (<2.6 cm), less than the 200th of the height. But a loss of the half of the stiffness of the cables generates a loss of 70 % of the grid shell rigidity. Without cables the stiffness of the grid shell is 10 times lower than with the 5 mm cables.

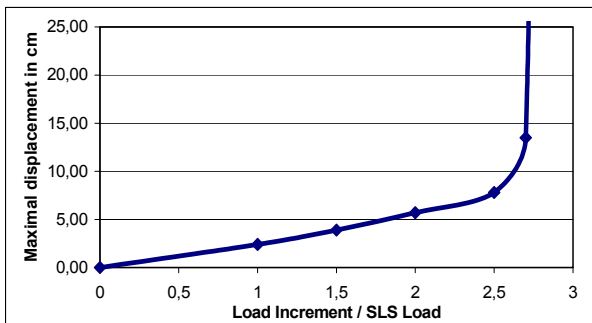


Figure 9: Maximal displacements

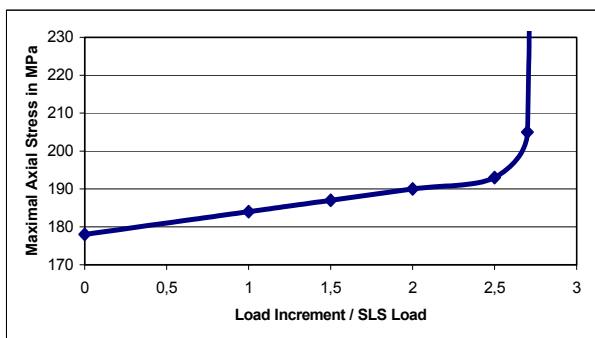


Figure 10: Maximal axial stresses

Furthermore it was necessary to test the stability of the grid shell and it was decided to increase the load until local buckling appears. Results are presented below. Figure 9 shows the maximal displacements in cm, figure 10 the maximal axial stresses in MPa

for every load increment with SLS load as reference. One can observe that buckling appears for higher loads than that of the ULS. One can thus conclude that this structure is safe. It is remarkable that, before buckling, the displacement and stresses variations are proportional to the load increment. The behaviour is thus linear elastic in a quite large range of loading. Moreover the increase in stresses in the beams is relatively low compared to the initial stresses (less than 15%).

6. CONCLUSIONS AND FURTHER WORK

In order to develop new fields of applications for composites in construction, proposals were made for a composite grid shell. The process of assembly of this type of structure was detailed. As the complexity of the modeling of the erection process required specific computer programs, the dynamic relaxation algorithm was presented and applied to flexible beams and grid shells. The quality and robustness of DR was shown through several examples for the form-finding and the structural analysis.

The last example demonstrated the feasibility of a composite grid shell. Standard glass fiber pulltruded tubes were used for the model of the grid and standard elements were used for joining the tubes. The stresses in the structure remain quite reasonable, so that this type of structure can be very efficient and economic for the construction of shelters for temporary or permanent purposes. However, it is worth reminding that this model of grid shell is still incomplete. Indeed the structure presented above is geometrically perfect and it is well known that imperfections induce a loss of rigidity on that type of structure. Therefore we will have in the future to introduce eccentricities at connecting nodes and to study the influence of those imperfections.

In order to fully demonstrate the structural efficiency of grid shells and their outstanding elegance, a large-scale model (10 m span) has been built in the ENPC and is today still under testing (Figure 11).



Figure 11: Experimental grid shell in the ENPC

7. REFERENCES

- [1] **Limam, O., Nguyen, V.T. and Foret, G.**, Numerical and experimental analysis of two-way slabs strengthened with CFRP strips, *Engineering Structures*, 27 (2005), p. 841-845
- [2] **Jülich, A. S., Caron, J.-F. and Baverel, O.**, Cable structure with load-adapting geometry, *3rd Int. Conf. for Composite in Construction*, (2005) p. 1103-1110
- [3] **Baverel, O., Nooshin, H. and Kuroiwa, Y.**, Configuration processing of nexorades using genetic algorithms, *Journal of the I.A.S.S.*, 45 n°2 (2004).
- [4] **Douthe, C., Baverel, O. and Caron J.-F.**, Propositions for a composite grid shell, Conception and structural analysis, *3rd Int. Conf. for Composite in Construction*, (2005) p. 1079-1086
- [5] Weald and Downland grid shell official web site: <http://www.wealddown.co.uk/downland-gridshell.htm>
- [6] **Hennicke, J., Matsushita, K., Otto, F. et al.**, Gitterschalen Grid shells, *Institut für Leichte Flächentragwerke (IL)*, (1974).
- [7] **Schek, H. J.**, The force density method for form-finding and computation of general networks, *Computer methods in applied mechanics and engineering*, 3 (1974), p. 115-134.
- [8] **Motro, R. and Maurin, B.**, The surface stress density method as a form-finding tool for tensile membranes, *Engineering Structure*, 20 (1998), p. 712-719.
- [9] **Day, A. S.**, An introduction to dynamic relaxation, *Engineer*, 219 (1965), p. 218-221.
- [10] **Barnes, M. R.**, Applications of dynamic relaxation to the design and analysis of cable, membrane, and pneumatic structures, *2nd Int. Conf. on Space Structure, Guilford* (1975).
- [11] **Barnes, M. R.**, Form-finding and Analysis of Tension Structures by Dynamic Relaxation, *International Journal of Space Structure*, 14 n°2 (1999).
- [12] **Adriaenssens, S., Barnes, M. R. and Williams, C.**, A new analytical and numerical basis for the form-finding and analysis of spline and grid-shell struct., in *B. Kumar and B. Topping ed., Computer Developments in civil and Structural Engineering* (1999) Edinburgh, Civil Comp Press, p.83-90.
- [13] **Han, S.-E. and Lee, K.-S.**, A study of the stabilising process of unstable structures by dynamic relaxation method, *Computer and Structure*, 81 (2003), p. 1677-1688.
- [14] **Sab, K., Alaoui, A. and Pradel, F.**, Molecular dynamics for the finite deformation of random elastic grids, *Mechanics of Materials* (2004).
- [15] **Papadrakakis, M.**, A method for the automatic evaluation of the dynamic relaxation parameters, *Computer. Methods in applied mechanics and engineering*, 25 (1981), p. 35-48.
- [16] More about Scilab™ release 3.1 on the official website, <http://scilabsoft.inria.fr/>